JACS
JOURNAL OF THE AMERICAN CHEMICAL SOCIETY
Article
pubs.acs.org/JACS

Vapor Pressure of Water Nanodroplets

Matías H. Factorovich,[†] Valeria Molinero,[‡] and Damián A. Scherlis*,[†]

[†]Departamento de Química Inorgánica, Analítica y Química Física/INQUIMAE, Facultad de Ciencias Exactas y Naturales, Universidad de Buenos Aires, Ciudad Universitaria, Pab. II, Buenos Aires, C1428EHA Argentina

[‡]Department of Chemistry, University of Utah, 315 South 1400 East, Salt Lake City, Utah 84112-0850, United States

Supporting Information

ABSTRACT: Classical thermodynamics is assumed to be valid up to a certain length-scale, below which the discontinuous nature of matter becomes manifest. In particular, this must be the case for the description of the vapor pressure based on the Kelvin equation. However, the legitimacy of this equation in the nanoscopic regime can not be simply established, because the determination of the vapor pressure of very small droplets poses a challenge both for experiments and simulations. In this article we make use of a grand canonical screening approach recently proposed to compute the vapor pressures of finite systems from molecular dynamics simulations. This scheme is applied to water droplets, to show that the applicability of the Kelvin equation extends to unexpectedly small lengths, of only 1 nm, where the inhomogeneities in the density of matter occur within spatial lengths of the same order of magnitude as the size of the object. While in principle this appears to violate the main assumptions underlying thermodynamics, the density profiles reveal, however, that structures of this size are still homogeneous in the nanosecond time-scale. Only when the inhomogeneity in the density persists through the temporal average, as it is the case for clusters of 40 particles or less, do the macroscopic thermodynamics and the molecular descriptions depart from each other.

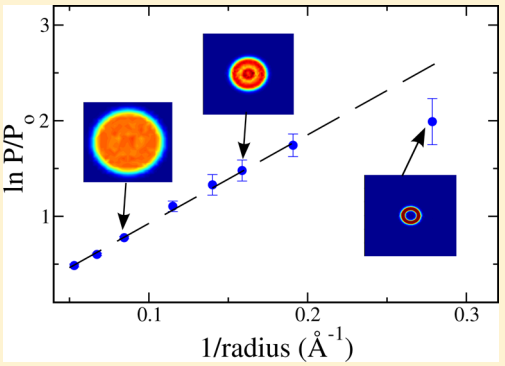

I. INTRODUCTION

In describing the physical properties of matter, there is a certain length-scale for which the assumptions of classical thermodynamics break down because the discrete nature of matter becomes manifest. How and when this transition takes place between the macroscopic and the nanoscopic domains is one of the most intriguing questions in statistical mechanics and in many areas within condensed and soft matter sciences.[1−4] The vapor pressure and the surface tension are two paradigmatic examples of those collective features that can not be grasped by a continuous thermodynamical approach when it comes to tiny droplets and nanoparticles.[5−7] Yet, the comprehension of these two properties is highly relevant, not only from a fundamental, chemical-physics standpoint, but also because they determine processes of central interest in materials engineering and catalysis,[1,3,8−11] as well as in environmental and atmospheric chemistry, where they appear as essential ingredients in classical nucleation theory (CNT).[12−14] In particular, an accurate assessment of the vapor pressure of nanoaggregates is not easily accessible via experiments, neither through calculations.[7] The Kelvin equation provides the vapor pressure (P_v) of a droplet as a function of the radius of curvature r of the interface:

$$\ln \frac{P_v}{P_0} = \frac{2\sigma}{r\rho RT} \quad (1)$$

where P_0 is the vapor pressure of the bulk substance, σ is the surface tension, ρ is the density of the condensed phase, R is the gas constant, and T is the temperature. For very small droplets of just a few nanometers of diameter, the effect of curvature on surface tension starts to be important. This can be accounted for through the Tolman equation[5]

$$\frac{\sigma}{\sigma_0} = \frac{1}{1 + 2\delta/r} \quad (2)$$

with σ_0 the surface tension of the planar interface, and δ the so-called Tolman length,[15] which assumes a characteristic value for every fluid. The combination of eqs 1 and 2 can in principle yield the dependence on radius of the vapor pressure. Nevertheless, as the diameter of the droplet approaches the nanometer scale, the validity of these expressions derived from classical thermodynamics becomes questionable. There has not been a general agreement regarding the limit of applicability of these equations. On the basis of thermodynamic arguments or numerical simulations, or even based on indirect experimental evidence, different authors, including Tolman himself, have situated it in disparate lengths, from only a few Å ngströms to some tens of nanometers.[5,7,16−25] This limit has been explored using Lennard-Jones potentials and molecular dynamics simulations with constant number of particles.[7,17−19,22] The

Received: May 29, 2013

   dx.doi.org/10.1021/ja405408n | J. Am. Chem. Soc. XXXX, XXX, XXX−XXX

vapor pressures computed using this route exhibit large uncertainties, due to the small number of particles in the vapor phase and to the infrequent collisions in the vapor.[17,18] Different approaches based on Monte Carlo simulations have been also applied to investigate this limit in the context of CNT, reporting that the deviations from the classical theory occur in a size range that goes from only four up to sixteen molecular diameters, depending on the interaction potential, the temperature, and the methodology.[23−25] Many studies have focused on the nucleation of small liquid droplets, aiming to estimate size distributions and the formation free energies of Lennard-Jones and water clusters as a function of temperature and supersaturation.[26−30] Zhukhovitskii devised a grand canonical molecular dynamics scheme to identify the critical cluster size of argon for different $T-P$ conditions.[26] To tackle the same problem, Kusaka and collaborators later proposed a coarse graining of the total volume in small compartments containing in average no more than one molecule or aggregate, with which they circumvented the issue of an arbitrary cluster definition.[27] Equilibrium distributions and free energies were evaluated in the grand canonical ensemble from the probability of finding a cluster of a given size in the coarse-grained volume. Soon after, this method was generalized by incorporating umbrella sampling and the potential energy as an order parameter, allowing to characterize the free energy surface of argon in terms of the number of particles and the energy of the aggregate.[28] Oh and Zeng implemented a canonical Monte Carlo methodology where a restriction was imposed on the maximum number of particles that a cluster can attain.[30] This strategy allows to sample a metastable situation that otherwise could not be observed, and was employed to determine the critical size and the formation free energy of argon clusters. A rather complete overview on theoretical and simulation aspects of the interfacial properties of nanoscopic liquid drops was recently offered in a topical review by Malijevský and Jackson.[31]

In this article, we employ a simple grand canonical screening (GCS) approach[32] to calculate the vapor pressure of water droplets in the range 1−4 nm diameter. This methodology, in combination with first-principles DFT molecular dynamics, allows us to assess the applicability and the limitations of the Kelvin equation, and to analyze at the molecular level the cause of its divergence with respect to the molecular description.

II. METHODOLOGY

A. Water Model. The mW coarse-grained model of water[33] was employed to complete the large number of grand canonical molecular dynamics simulations necessary to obtain the vapor pressure curves reported in the next section. The mW potential reproduces the energetics, density, and structure of liquid and solid water and its phase transitions, with comparable or better accuracy than most atomistic models, at nearly 1% of the computational cost.[33] This model represents each molecule as a single particle interacting through anisotropic short-ranged potentials that encourage "hydrogen-bonded" water structures. It adopts the short-ranged interaction form of the Stillinger-Weber force-field, which consists of a sum of two-body attraction terms favoring high coordination, and three-body repulsion terms reinforcing tetrahedral hydrogen-bonded configurations.[33] In recent years, the mW model has been repeatedly applied to explain the behavior of water in various conditions and regimes (see for example ref 34 and references therein).

B. Molecular Dynamics Simulations. In this study, molecular dynamics simulations were performed in the canonical and grand canonical ensemble. Grand canonical molecular dynamics (GCMD) schemes introduce Metropolis Monte Carlo sampling throughout the dynamical evolution to allow for particle exchange with a reservoir, hence preserving a temporal description at a controlled chemical potential. The movement of the particles is ruled by the integration of the Newton equations using the Verlet algorithm at constant temperature, which is controlled with the Nosé-Hoover thermostat. Insertion and deletion attempts are effected on single particles with equal probability and anywhere in the box, adopting the usual acceptance criteria of the Monte Carlo grand-canonical algorithm and assuming the vapor is an ideal gas.[35,36] Along the grand canonical dynamics, a number of attempts for particle insertion and deletion are carried at every time-step: this number is the so-called GC/MD ratio. It is desirable to keep this parameter as low as possible to minimize computer time, but in turn it must be high enough to ensure that the target chemical potential is reached during the simulation.[37,38] GC/MD ratios in the range 20−100 have been typically used in previous studies.[37−39] In our simulations a GC/MD ratio of 20 was adopted, which is common in the literature and gives converged results for the systems examined here. GCMD simulations were performed using a properly modified version of the LAMMPS program.[40]

Classical and first-principles molecular dynamics of water were performed to construct the density maps and density profiles. Classical molecular dynamics were realized using the LAMMPS program, with the same time-step as employed in the GCMD simulations, equal to 5 fs. On the other hand, first-principles dynamics were based on density functional theory and the Car−Parrinello method,[41] as implemented in the public package Quantum-Espresso.[42] These simulations were performed in the microcanonical ensemble using a time-step of 0.19 fs, adopting the PW91 exchange-correlation functional,[43,44] Vanderbilt ultrasoft pseudopotentials,[45] and a cutoff of 25 Ry on the plane-waves basis set.

C. Calculation of the Vapor Pressure: the GCS Approach. The grand canonical screening procedure to compute the vapor pressure is described in detail in reference.[32] In the following, we give a brief overview of the technique. According to classical nucleation theory,[14] for a given supersaturation or chemical potential μ, a critical cluster size N^* exists involving a saddle point in the free energy surface. The vapor pressure of such a cluster is related to this chemical potential by $\mu_{eq} = \mu^{\theta} + RT \ln(P_v/P_{\theta})$. In the present approach, to determine P_v for a nanodroplet of size N, independent grand canonical simulations must be conducted, each one at a different chemical potential. As the simulation evolves, the total number of molecules may rise or drop, depending on whether the magnitude of μ is, respectively, above or below the equilibrium value μ_{eq} associated with that N. For example, if the value of μ fixed in the simulation is above the value of μ_{eq} corresponding to the initial curvature of the interface (determined by N), condensation occurs leading to an increase in radius, which in turn diminishes the magnitude of μ_{eq}. In this way μ_{eq} experiences a gradual decrease, moving away from μ, and thus the growth of the droplet continues until the simulation box is completely filled. Conversely, if μ is below μ_{eq} at the beginning of the simulation, the evaporation proceeds until all particles have disappeared. By repeating this computational experiment for a given N at different chemical potentials,

dx.doi.org/10.1021/ja405408n | J. Am. Chem. Soc. XXXX, XXX, XXX−XXX

an upper and a lower bound can be established for μ_{eq}. The uncertainty in P_v is then determined by the lower and upper values of μ producing, respectively, the condensation and evaporation of the droplet. It must be noted, though, that as the chemical potential gets closer to μ_{eq} the ratio between particles insertion and deletion tends to 1, implying that longer simulations are required to discern between evaporation and condensation. The error can hence be reduced at the expense of computational time.[32]

In the case of very small clusters in the vicinity of the equilibrium pressure, namely below 50 particles, the final evaporation or condensation behavior is not uniquely determined by the chemical potential but may depend on "hidden variables" as the initial structure of the cluster, the sequence of random numbers in the Monte Carlo run, or the assignment of initial velocities from the Boltzmann distribution. In other words, at the same chemical potential, two independent trajectories corresponding to nanodroplets of the same size might evolve distinctly to evaporation or to condensation. This ambiguous behavior is only observed for small N and follows from the fact that the stochastic components of the computational experiment become more important as the number of particles decreases. This is not a serious problem as far as it is recognized and can be handled by performing for each value of the chemical potential, a set of several short trajectories, each one based on a different sequence of random numbers or departing from different initial configurations and velocities. In particular, μ_{eq} is chosen as the value originating evaporation and condensation trajectories with equal probability. The error bar for that data-point can be similarly estimated on the basis of condensation and evaporation probabilities. Here, 10 trajectories were performed for each data-point for $N \leq 94$, with the exception of $N = 9$ at the two highest temperatures, for which 25 trajectories were considered. The lower bound for the uncertainty was chosen as the pressure for which the number of trajectories leading to condensation was larger than 20%. Similarly, the upper bound was given by the pressure above which the evaporation probability (or, equivalently, the number of trajectories producing evaporation) was less than 20%. Further details on the computation of the errors can be found in the supporting material.

We have shown in ref 32 that the GCS procedure described above reproduces the vapor pressure of bulk water and argon with a slightly better precision than the Gibbs-ensemble approach. Moreover, we have computed the relative vapor pressure for water aggregates of size ~2 nm using both the mW and the SPC/E models to find that the two force-fields lead to the same results.[32]

III. RESULTS AND DISCUSSION

We applied the GCS procedure to determine the vapor pressure of water aggregates of different sizes, from only 9 molecules up to 960. Figure 1 presents the logarithm of the relative vapor pressure obtained from GCMD simulations with the mW model at three temperatures as a function of the inverse radius, compared with the results given by the Kelvin equation. This data is also summarized in Table 1. Strikingly, the thermodynamic formula reproduces the simulations for radii as small as 7 Å with discrepancies below 5% at 278 K, and even smaller for higher temperatures. For 298 and 318 K, the Kelvin equation predicts the vapor pressure of water aggregates

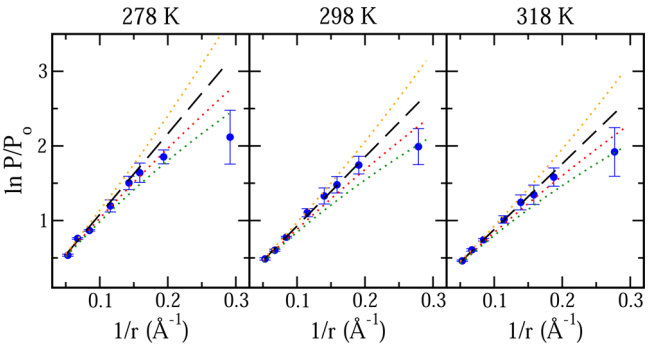

Figure 1. Logarithm of the relative vapor pressure of water nanodroplets as a function of the inverse radius. Blue circles: grand canonical screening results. The dashed and dotted lines show the predictions of the Kelvin equation for different Tolman lengths. Black: $\sigma = \sigma_0$ ($\delta = 0$). Orange: $\delta = -0.5$ Å. Red: $\delta = 0.5$ Å. Green: $\delta = 1.0$ Å.

with extraordinary accuracy all the way down to systems composed of just 37 molecules, or nearly 1.2 nm of diameter.

The approximation shows discrepancies of up to 20%, depending on temperature, for the cluster of 20 particles, and definitely breaks for the one of 9 molecules, which exhibits strong negative deviations for all three temperatures.

The magnitude and even the sign of the Tolman length (δ) appearing in eq 2 has for long been a matter of debate, but there is agreement that it must be of the order of the intermolecular distances.[15,31,46−55] For water, the value originally proposed by Tolman was 1 Å,[15] with many subsequent estimations from theory and simulations falling close to this former appraisal.[48−52] The validity of these estimations has nevertheless been disputed by a number of studies claiming that the surface tension must increase with curvature (which implies $\delta < 0$),[47,54,55] with a recent work based on molecular dynamics simulations reporting for the TIP4P/2005 water model a negative value of −0.56 Å.[56] On the other hand, the assessment of δ on the basis of experimental data typically involves a number of assumptions and is technically challenging, and this explains why consensus has not been met either among experimentalists, who reported Tolman lengths for water ranging from −0.47 to +0.6 Å.[57,58] Whereas the curvature dependence of the surface tension and the sign of the Tolman length remain controversial, there is general agreement on the following: it must be very small in magnitude, it depends on droplet size and temperature (presumably decreasing with T), and its physical meaning is lost when going to very small systems, in the order of a few molecular diameters.[31,51,53] In this context, it is remarkable that the Kelvin equation matches our data with a Tolman length of approximately zero until the cluster size reaches about 4 molecular diameters, with an abrupt failure below that range.

Such a good performance of the thermodynamic formulation to describe these small objects may seem unexpected. In fact, the Kelvin equation turns out to be valid in a region where the inhomogeneities in the density of matter occur within spatial lengths of the same order of magnitude as the size of the aggregate, whereas among the major assumptions underlying the thermodynamic treatment, there are (i) the homogeneity of the surface and the continuous nature of the fluid, (ii) a constant density inside the droplet, independent from radius, and (iii) the sphericity of the aggregate. Clearly, these requirements do not hold for the instantaneous configurations of clusters consisting of less than a few hundred molecules, as

dx.doi.org/10.1021/ja405408n | J. Am. Chem. Soc. XXXX, XXX, XXX−XXX

Table 1. Relative Vapor Pressures (P_v/P_0) and Radii (r, in Å) for Different Water Droplets Composed by N Molecules[a]

	278 K		298 K		318 K	
N	r	P_v/P_0	r	P_v/P_0	r	P_v/P_0
9	3.43	8.31 (3.61)	3.59	7.35 (1.96)	3.61	6.82 (2.63)
20	5.16	6.38 (0.62)	5.24	5.71 (0.72)	5.33	4.87 (0.64)
37	6.30	5.15 (0.63)	6.30	4.39 (0.51)	6.32	3.84 (0.53)
51	7.00	4.50 (0.42)	7.14	3.78 (0.39)	7.19	3.47 (0.34)
94	8.66	3.31 (0.27)	8.69	3.02 (0.14)	8.74	2.76 (0.23)
237	11.81	2.38 (0.02)	11.84	2.18 (0.02)	11.84	2.10 (0.03)
471	14.85	2.14 (0.02)	14.86	1.82 (0.02)	14.90	1.83 (0.03)
960	18.86	1.70 (0.02)	18.88	1.62 (0.02)	18.90	1.58 (0.02)

[a]Absolute errors are given in parentheses. The values of P_0 for the mW model at 278, 298, and 318 K, are, respectively, 0.13 mbar, 0.49 mbar and 1.50 mbar.

can be seen in Figure 2, and as reflected in the nonequal eigenvalues of the moment of inertia tensor, presented in the

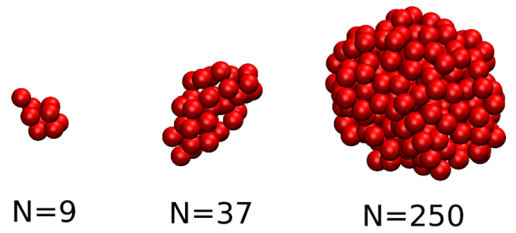

Figure 2. Instantaneous configurations of water clusters of different sizes, randomly selected from the molecular dynamics simulations at 298 K. The shape deviation from sphericity is significant for systems with less than 150 particles.

Supporting Information. Interestingly, however, they do hold for the temporal averages of their trajectories, displayed in the density maps of Figure 3. Since the thermodynamic properties are manifestations of the behavior averaged in the macroscopic time-scale, it can be argued that the master equations remain valid for those systems in which the dynamics smoothes down the discrete, inhomogeneous structure of the nanoaggregate. Figures 3 and 4 show that droplets of 1.2 nm diameter or larger reasonably fit into this premise: they all exhibit a spherical shape and a constant density along the most part of the condensed phase, equal to 0.033 Å^{-3}, which is the density of bulk water. Smaller droplets depart from this paradigm: the averaged density is not homogeneous, but presents a peak on the boundary, while the sphericity is lost in shorter time lengths. Coincidentally, the agreement between the Kelvin equation and the simulations deteriorates at the same point

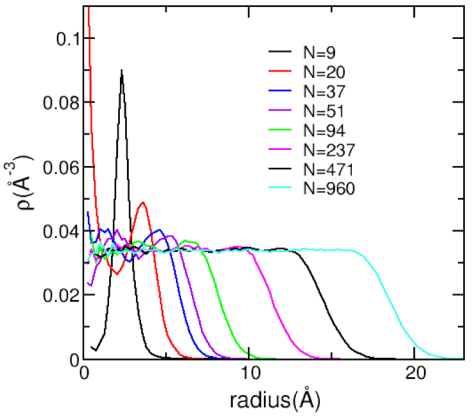

Figure 4. Time-averaged radial density profiles of water droplets of different sizes at 298 K. The averaging was performed on NVT molecular dynamics trajectories extended for at least 3 ns.

where the averaged density profile of the cluster starts to become strongly inhomogeneous.

The effect of rotations on the density distributions were checked by aligning the eigenvectors of the moment of inertia tensors at each step of the molecular trajectories. No appreciable differences were found when rotation was taken into account, presumably because the liquid-like nature of these clusters at room temperature produces continuous deformations in which the rotational and the internal degrees of freedom are too much coupled. The particular density distribution observed for the smallest clusters has been corroborated in the case of the 9 molecules aggregate by means of ab initio molecular dynamics simulations (Figure 5),

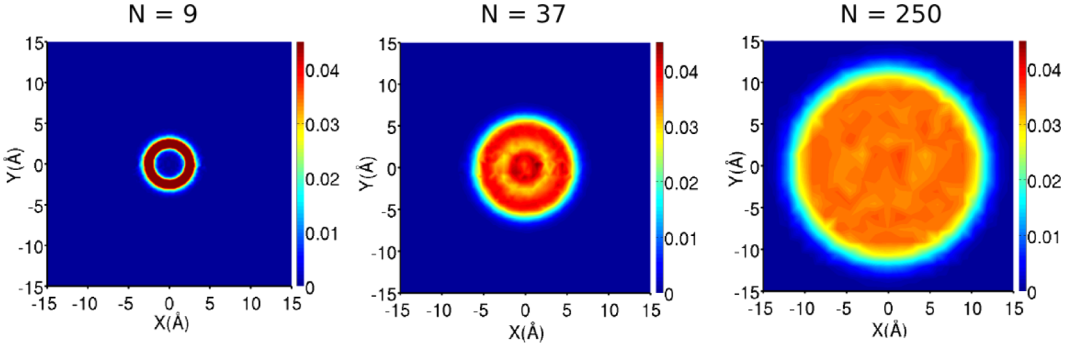

Figure 3. Bidimensional density maps of water droplets of different sizes at 298 K. Units for the color scale bar are Å^{-3}. The densities were averaged over time-windows of 100 ns for the smaller systems and 3 ns for the largest.

dx.doi.org/10.1021/ja405408n | J. Am. Chem. Soc. XXXX, XXX, XXX−XXX

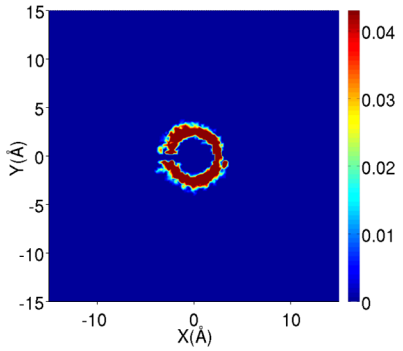

Figure 5. Same as Figure 3, obtained for the droplet of 9 molecules from ab initio molecular dynamics. The nonuniform density distribution is due to an insufficient averaging time of 20 ps.

which show that it is not an artifact of the mW potential. The agreement between the classical and the DFT ab initio calculations stems from the fact that both the mW and the DFT dynamics explore the same minima in phase space. Figure 6 presents some representative instantaneous configurations

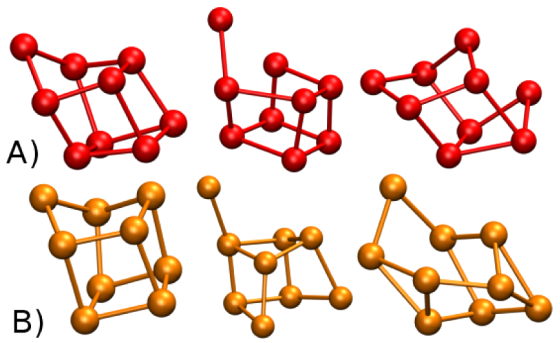

Figure 6. Different configurations of a cluster of 9 water molecules, taken from quantum (A) and classical (B) molecular dynamics simulations, based on DFT and on the mW model, respectively. For the sake of comparison, only the oxygen atoms are depicted. Bars are indicative of two atoms lying at less than 3.4 Å, which is the distance between two water molecules forming an H-bond. The first image of the series predominates along the dynamics in both approaches.

extracted from the classical and the quantum dynamics. Both approaches produce the same structures, typically showing a molecule in each one of the eight corners of a cube, plus a ninth molecule off an edge. These geometries turn out to be coincidental with the ab initio minimum energy configurations of the cluster of 9 water molecules reported in the literature.[59,60] Therefore, we would not expect a substantial improvement if the mW potential were to be replaced by an atomistic or even a quantum-mechanical treatment: the resulting vapor pressure is ultimately determined by the magnitude of the intermolecular interactions, which classical water force-fields are fitted to reproduce pretty accurately, sometimes even better than obtained via first-principles simulations (for example, within DFT-GGA the solid−liquid transition temperature in water is off by around 140 K[61]).

Estimates to the vapor pressure of water nanodroplets can be obtained from the literature related to classical nucleation theory. Kusaka and collaborators applied a grand canonical methodology to evaluate equilibrium distributions and free energies of SPC/E water.[27] The maxima in the free energy curves of Figure 7 gives the critical cluster sizes,[27] in fair agreement with our own results. For example, for a supersaturation $P/P_0 \approx 5$ at 298 K the critical cluster has approximately 35 molecules, whereas for the same temperature we find $P_v/P_0 = 4.39$ for an aggregate of 37 mW molecules (Table 1). The critical sizes are slightly overestimated in Kusaka's method with respect to our approach, this overestimation becoming more notorious for higher supersaturations. The small discrepancies are attributable to the different methodologies and, to a lesser extent, to the distinct potentials (in previous work[32] we showed that both the SPC/E and the mW models give very similar relative vapor pressures for a cluster of 94 molecules). The dynamical nucleation theory by Schenter et al. provides a different route to the vapor pressure of water clusters, based on the ratio between the evaporation and the condensation rates.[62,63] Figure 3 of ref 62 shows for $P/P_0 = 10$ that the rate constants α_i and β_{i-1} reach the same value for droplets of slightly above 40 molecules. The GCS procedure predicts a P/P_0 ratio close to 5.2 for clusters of this size at 278 K. The classical Kelvin equation, in turn, gives a relative vapor pressure of nearly 5.6, meaning that while our approach yields negative deviations from the Kelvin equation, the dynamical nucleation theory technique would show positive deviations. Part of this disagreement might be ascribed to differences in temperature and force fields: simulations in ref 62 have been performed at 243 K with a polarizable water model. Beyond this particular result, it must be noticed that methods based on CNT are designed to predict the evaporation and condensation rates for a distribution of nanoaggregates of different sizes in dynamical equilibrium. Our approach, instead, considers a single droplet (or interface) in equilibrium with the vapor phase, but isolated from any other cluster or interface. This is the same situation described by the Kelvin equation, which may explain why it shows a closer agreement with our results. A full accord between the two methodologies should then not be expected. The dynamical nucleation theory is a more powerful approach since it gives information on a full distribution of clusters. Moreover, CNT schemes provide evaporation and condensation rates, which in GCMD would require a careful validation to ensure that time-evolution is quantitatively realistic. On the other hand, dynamical CNT techniques rely on more assumptions and parameters than our approximation, which depends only on the force-field, and therefore we expect it to be more accurate to predict the relative vapor pressure of an isolated nanodroplet. In those CNT applications where, at variance with dynamical nucleation theory, aggregates are envisioned as independent entities in the vapor phase, with no connection with clusters of other sizes, the framework of a dynamical exchange of particles between a distribution of droplets of different sizes is lost, and the critical cluster size for a given supersaturation has to be consistent with the one predicted from our analysis. Possibly, the present treatment may be used in a complementary way to classical nucleation theory methods, by providing values for the vapor pressures of clusters that can be exploited in larger-scale models.

Our approach to the vapor pressure of clusters is conceptually analogous to the one followed by Zhukhovitskii to estimate critical sizes.[26] In that work, a grand canonical molecular dynamics scheme was proposed where the insertion of molecules takes place at random positions on the system boundary with velocities chosen from the Maxwell−Boltzmann distribution, removing at the same time any molecule coming from the simulation cell and traveling across this boundary.[26] In this way, the algorithm reproduces a vapor environment

dx.doi.org/10.1021/ja405408n | J. Am. Chem. Soc. XXXX, XXX, XXX−XXX

corresponding to a desired temperature and pressure. To identify the critical cluster size for different conditions, the number of particles N was monitored as a function of time at a fixed pressure and temperature, starting from different cluster sizes. Two possibilities were observed for these trajectories: evaporation or condensation, meaning respectively that the initial size was below or above the critical value. This behavior is analogous to the one observed in the GCS simulations, with the only distinction that in our work different chemical potentials were screened for a given initial size to determine the vapor pressure, whereas Zhukhovitskii screened different initial values of N for a fixed pressure to obtain the critical size. Nevertheless, the two approaches are equivalent and provide access to the same information, i.e., the size of the metastable cluster associated with a given vapor pressure. The molecular dynamics method proposed in ref 26 is likely to be better suited to examine weakly interacting fluids as the Lennard-Jones model, for which small clusters are difficult to stabilize in a more conventional grand canonical framework. On the other hand, our approach seems more appropriate for systems exhibiting a low vapor pressure as water, where the application of Zhukhovitskii's scheme would require very large simulation cells and long sampling times to ensure a reasonable exchange of particles in the vapor phase that provides a converged statistics.

IV. FINAL REMARKS

In summary, we have determined the vapor pressure of water nanodroplets from 9 to 960 molecules. The results led us to conclude that the Kelvin equation is valid as far as the temporally averaged density of the water droplets exhibit a homogeneous profile, which establishes a link between time and the basic assumptions behind any thermodynamic approach. This is in fact the case for droplets as small as 0.6 nm radius at 278 K or even smaller at higher temperatures. For water, this implies a radius of only two molecular diameters, which is much smaller than the limit of around 10 molecular diameters for which the capillary approximation is considered to be valid in the literature.[31] A question remains on the universality of the present conclusions, specially their connotation for other nanosystems exhibiting different structure and interactions strength. This topic will be the subject of future investigations.

■ ASSOCIATED CONTENT

Ⓢ Supporting Information

Plots of the pressure-dependent evolution of the number of molecules as a function of simulation step for clusters of 94, 37, and 9 molecules; the eigenvalues of the moment of inertia tensor for various clusters; the definition of the nanodroplet radii; details on cell size and starting configurations, and on the calculation of the error for small clusters. This material is available free of charge via the Internet at http://pubs.acs.org.

■ AUTHOR INFORMATION

Corresponding Author

damian@qi.fcen.uba.ar

Notes

The authors declare no competing financial interest.

■ ACKNOWLEDGMENTS

We thank Prof. Ernesto Marceca and Dr. Damian Bikiel for valuable discussions. We are also grateful to the reviewers for worthy comments. This study has been supported by a collaborative grant of the Agencia Nacional de Promocion Cientifica y Tecnologica de Argentina, PICT 2007-2111 V.M. and D.A.S. We acknowledge the Center of High Performance Computing of the University of Utah for the allocation of computing time.

■ REFERENCES

(1) Katsoulakis, M. A.; Vlachos, D. G. *Phys. Rev. Lett.* **2000**, *84*, 1511−1514.
(2) Castleman, A. W., Jr.; Keese, R. G. *Science* **1988**, *241*, 36−42.
(3) Rajamani, S.; Truskett, T. M.; Garde, S. *Proc. Natl. Acad. Sci. U.S.A.* **2005**, *102*, 9475−9480.
(4) Gross, D. H. E. *Microcanonical Thermodynamics: Phase Transitions in 'Small' Systems*, 1st ed.; World Scientific Pub. Co. Inc.: Singapore, 2001.
(5) Tolman, R. C. *J. Chem. Phys.* **1949**, *17*, 333−337.
(6) Adamson, A. W.; Gast, A. P. *Physical Chemistry of Surfaces*, 6th ed.; Wiley-Interscience: New York, 1997.
(7) Fujikawa, S.; Yano, T.; Watanabe, M. *Vapor Liquid Interfaces, Bubbles and Droplets. Fundamentals and Applications*; Springer-Verlag: Berlin, 2011.
(8) Peeters, P.; Hrubý, J.; van Dongen, M. E. H. *J. Phys. Chem. B* **2001**, *105*, 11763−11771.
(9) Kodambaka, S.R. M. C.; Tersoff, J.; Ross, F. M. *Science* **2007**, *316*, 729−732.
(10) Kuna, J. J.; Voitchovsky, K.; Singh, C.; Jiang, H.; Mwenifumbo, S.; Ghorai, P. K.; Stevens, M. M.; Glotzer, S. C.; Stellacci, F. *Nat. Mater.* **2009**, *8*, 837−842.
(11) Choi, S.; Jamshidi, A.; Seok, T. J.; Wu, M. C.; Zohdi, T. I.; Pisano, A. P. *Langmuir* **2012**, *28*, 3102−3111.
(12) Rodebush, W. H. *Proc. Natl. Acad. Sci. U.S.A* **1954**, *40*, 789−794.
(13) Andreae, M. O. *Science* **2013**, *339*, 911−912.
(14) Zhang, R.; Khalizov, A.; Wang, L.; Hu, M.; Xu, W. *Chem. Rev.* **2012**, *112*, 1957−2011.
(15) Tolman, R. C. *J. Chem. Phys.* **1949**, *17*, 118−127.
(16) Kalikmanov, V. I. *J. Chem. Phys.* **2008**, *129*, 44510.
(17) Thompson, S. M.; Gubbins, K. E. *J. Chem. Phys.* **1984**, *81*, 530−542.
(18) Shreve, A. P.; Walton, J. P. R. B.; Gubbins, K. E. *J. Chem. Phys.* **1986**, *85*, 2178−2186.
(19) Nijmeijer, M. J. P.; Bruin, C.; van Woerkom, A. B.; Bakker, A. F.; van Leeuwen, J. M. J. *J. Chem. Phys.* **1992**, *96*, 565−576.
(20) Fisher, L. R.; Israelachvili, J. N. *J. Colloid Interface Sci.* **1981**, *80*, 528−541.
(21) Samsonov, V. M.; Shcherbakov, L. M.; Novoselov, A. R.; Lebedev, A. V. *Colloids Surf.* **1999**, *160*, 117−121.
(22) Moody, M. P.; Attard, P. *Phys. Rev. Lett.* **2003**, *91*, 56104.
(23) Neimark, A. V.; Vishnyakov, A. *J. Chem. Phys.* **2005**, *122*, 174508.
(24) Merikanto, J.; Zapadinsky, E.; Lauri, A.; Vehkamäki, H. *Phys. Rev. Lett.* **2007**, *98*, 145702.
(25) Nellas, R. B.; Keasler, S. J.; Siepmann, J. I.; Chen, B. *J. Chem. Phys.* **2010**, *132*, 164517.
(26) Zhukhovitskii, D. I. *J. Chem. Phys.* **1995**, *103*, 9401−9407.
(27) Kusaka, I.; Wang, Z.-G.; Seinfeld, J. H. *J. Chem. Phys.* **1998**, *108*, 3416−3423.
(28) Kusaka, I.; Oxtoby, D. W. *J. Chem. Phys.* **1999**, *110*, 5249−5261.
(29) Oh, K. J.; Gao, G. T.; Zeng, X. C. *J. Chem. Phys.* **1998**, *109*, 8435−8441.
(30) Oh, K. J.; Zeng, X. C. *J. Chem. Phys.* **1999**, *110*, 4471−4476.
(31) Malijevský, A.; Jackson, G. *J. Phys.-Condens. Mater.* **2012**, *24*, 464121.

(32) Factorovich, M.; Molinero, V.; Scherlis, D. A. *J. Chem. Phys.* **2014**, *140*, 064111.
(33) Molinero, V.; Moore, E. B. *J. Phys. Chem. B* **2009**, *113*, 4008−4016.
(34) Moore, E. B.; Molinero, V. *Nature* **2011**, *479*, 506−508.
(35) Frenkel, D.; Smit, B. *Understanding Molecular Simulation*, 2nd ed.; Academic Press: San Diego, CA, 2002.
(36) Papadopoulou, A.; Becker, E. D.; Lupkowski, M.; van Swol, F. *J. Chem. Phys.* **1993**, *98*, 4897.
(37) Heffelfinger, G. S.; van Swol, F. *J. Chem. Phys.* **1994**, *100*, 7548−7552.
(38) Arya, G.; Chang, H.-S.; Maginn, E. J. *J. Chem. Phys.* **2001**, *115*, 8112.
(39) Cracknell, R. F.; Nicholson, D.; Quirke, N. *Phys. Rev. Lett.* **1995**, *74*, 2463−2466.
(40) Plimpton, S. *J. Comput. Phys.* **1995**, *117*, 1−19.
(41) Car, R.; Parrinello, M. *Phys. Rev. Lett.* **1985**, *55*, 2471.
(42) Giannozzi, P.; et al. *J. Phys.-Condens. Matter* **2009**, *21*, 395502.
(43) Perdew, J. P.; Wang, Y. *Phys. Rev. B* **1992**, *45*, 13244.
(44) Perdew, J. P.; et al. *Phys. Rev. B* **1992**, *46*, 6671.
(45) Vanderbilt, D. *Phys. Rev. B* **1990**, *41*, 7892.
(46) Lei, Y. A.; Bykov, T.; Yoo, S.; Zeng, X. C. *J. Am. Chem. Soc.* **2005**, *127*, 15346−15347.
(47) van Giessen, A. E.; Blokhuis, E. M. *J. Chem. Phys.* **2009**, *131*, 164705.
(48) Samsonov, V.; Bazulev, A.; Sdobnyakov, N. *Cent. Eur. J. Phys.* **2003**, *3*, 474−484.
(49) Samsonov, V. M.; Bazulev, A. N.; Sdobnyakov, N. Y. *Dokl. Phys. Chem.* **2003**, *389*, 83−85.
(50) Lu, H. M.; Jiang, Q. *Langmuir* **2005**, *21*, 779−781.
(51) Graziano, G. *Chem. Phys. Lett.* **2010**, *497*, 33−36.
(52) Xue, Y.-Q.; Yang, X.-C.; Cui, Z.-X.; Lai, W.-P. *J. Phys. Chem. B* **2011**, *115*, 109−112.
(53) Horsch, M.; Hasse, H.; Shchekin, A. K.; Agarwal, A.; Eckelsbach, S.; Vrabec, J.; Müller, E. A.; Jackson, G. *Phys. Rev. E* **2012**, *85*, 031605.
(54) El Bardouni, H.; Mareschal, M.; Lovett, R.; Baus, M. *J. Chem. Phys.* **2000**, *113*, 9804.
(55) Tröster, A.; Oettel, M.; Block, B.; Virnau, P.; Binder, K. *J. Chem. Phys.* **2012**, *136*, 064709.
(56) Joswiak, M. N.; Duff, N.; Doherty, M. F.; Peters, B. *J. Phys. Chem. Lett.* **2013**, *4*, 4267−4272.
(57) Holten, V.; Labetski, D. G.; van Dongen, M. E. H. *J. Chem. Phys.* **2005**, *123*, 104505.
(58) Azouzi, M. E. M.; Ramboz, C.; Lenain, J.-F.; Caupin, F. *Nat. Phys.* **2013**, *9*, 38−41.
(59) Maheshwary, S.; Patel, N.; Sathyamurthy, N.; Kulkarni, A. D.; Gadre, S. R. *J. Phys. Chem. A* **2001**, *105*, 10525−10537.
(60) Shields, R. M.; Temelso, B.; Archer, K. A.; Morrell, T. E.; Shields, G. C. *J. Phys. Chem. A* **2010**, *114*, 11725−11737.
(61) Yoo, S.; Zeng, X. C.; Xantheas, S. S. *J. Chem. Phys.* **2009**, *130*, 221102.
(62) Schenter, G. K.; Kathmann, S. M.; Garrett, B. C. *J. Chem. Phys.* **2002**, *116*, 4275−4280.
(63) Schenter, G. K.; Kathmann, S. M.; Garrett, B. C. *Phys. Rev. Lett.* **1999**, *82*, 3484−3487.